Glass transition of two-component liquids. II. The Lamb-Mössbauer factors

J. S. Thakur and J. Bosse
Institut für Theoretische Physik, Freie Universität Berlin, Arnimallee 14, D-1000 Berlin 33, Germany
(Received 6 February 1990)

The wave-number-dependent Lamb-Mössbauer factors (LMF's) of big and small particles in a glass of neutral hard spheres are investigated within mode-coupling theory by varying size ratio δ, total packing fraction η, and concentration c_1. It is possible to form a glass by the big particles only, while the small particles retain their mobility. Diffusion blocking of small particles is achieved by increasing either η or δ. The wave-number dependence of the small particles' LMF shows characteristic deviations from a Gaussian in contrast to big particles' LMF, which is almost Gaussian.

I. INTRODUCTION

The idea of Leutheusser[1] and Bengtzelius and Götze and Sjölander[2] to relate the liquid-glass transition to a zero-frequency pole emerging from the density-relaxation spectrum has been exploited continuously[3–10] to understand the dynamics of supercooled liquids and their critical behavior at the transition point. In all these papers, the well-known mode-coupling theory (MCT) has been employed. Several important implications of MCT on the liquid-glass transition have been confirmed by a hydrodynamic approach[11] and by molecular-dynamics simulations.[12,13] Most of these attempts have been on the freezing of *one-component* systems, however, in which localization of all particles of the system is associated with the arrest of density fluctuations, i.e., both coherent and incoherent density relaxation functions acquire a nonzero long-time limit signaling a transition to the nonergodic glass state. Many interesting physical phenomena like the percolation problem or the conductor-nonconductor transition in ionic glasses cannot be investigated within these models. Therefore, it has been suggested[9] to study multicomponent systems and to look for the tagged-particle motion. In this paper we will investigate Lamb-Mössbauer factors (LMF's) for binary mixtures of small and big particles within MCT. The theory requires nonergodicity parameters $f_{ss'}(q)$ and static structure factors as input, which is provided by our previous paper (referred to as paper I in the following).

The paper is organized as follows. In Sec. II we define the nonergodicity parameters as the $t=\infty$ limit of the density-relaxation function of a tagged particle. Using the expression of double differential scattering cross section the nonergodicity parameters are recognized as the LMF's of the system. The approximate way to calculate these LMF's is provided by MCT, which generates a self-consistent method for LMF's. These LMF's are calculated by varying η, δ, and c_1 of the system. The results are presented in Sec. III. In Sec. IV we give a summary and conclusions.

II. FORMAL FRAMEWORK

A. Tagged-particle density-relaxation function

Following the notation of paper I we define the tagged-particle density-relaxation function for a particle of species s as

$$\phi_s(q,t)=\frac{1}{N_s}\sum_{1\le j\le N_s}\langle e^{i\mathbf{q}\cdot\mathbf{r}_j^s(t)}e^{-i\mathbf{q}\cdot\mathbf{r}_j^s(0)}\rangle$$
$$=(\hat{N}_s^0(\mathbf{q})|e^{-i\mathcal{L}t}|\hat{N}_s^0(\mathbf{q}))\ , \tag{1}$$

with the normalized tagged-particle density of species s

$$\hat{N}_s^0(\mathbf{q})=\exp(-i\mathbf{q}\cdot\mathbf{r}_1^s)\sqrt{k_BT}\ . \tag{2}$$

$\phi_s(q;t)$ describes the density distribution of a tagged particle at time $t>0$, which was placed into the origin at $t=0$. From linear-response theory one finds

$$\langle N_s^0(\mathbf{q})\rangle_t=\phi_s(q;t)\ , \tag{3}$$

where $\phi_s(q=0,t)=1=\phi_s(q,t=0)$. Consequently, the long-time limit

$$f_s(q)=\lim_{t\to\infty}\phi_s(q,t)=(\hat{N}_s^0(\mathbf{q})|\mathcal{P}_0(\mathcal{L})|\hat{N}_s^0(\mathbf{q}))\ , \tag{4}$$

viz, $f_s(r)=V^{-1}\sum_{\mathbf{q}}e^{i\mathbf{q}\cdot\mathbf{r}}f_s(q)$ determines the probability of finding a tagged particle at finite distance r from its initial position after a long time $t\to\infty$. Accordingly, we talk about a delocalized or localized particle depending upon whether $f_s(q)=0$ or $\neq 0$.

B. Experimental relevance of $f_s(q)$: Lamb-Mössbauer factors

The scattering cross section for incoherent scattering is

$$\left.\frac{d^2\sigma}{d\Omega d\omega}\right|^{\text{incoh}}\propto\int_{-\infty}^{\infty}dt e^{i\omega t}\sum_s|b_s^{\text{incoh}}|^2\Psi^s(q,t)\sum_{1\le j\le N_s}\langle e^{-i\mathbf{q}\cdot\mathbf{r}_j^s(t)}e^{i\mathbf{q}\cdot\mathbf{r}_j^s}\rangle\ , \tag{5}$$

where $b_s^{\rm incoh}$ denotes the incoherent scattering length and $\Psi^s(q,t)$ describes the internal dynamics of the target particles. The long-time limit of the tagged-particle relaxation function thus determines the intensity of recoilless incoherent scattering:[14]

$$\left.\frac{d^2\sigma}{d\Omega d\omega}\right|_{\rm recoilless}^{\rm incoh} \propto \sum_s N_s |b_s^{\rm incoh}|^2 \Psi^s(\mathbf{q},\omega) f_s(\mathbf{q}) \ . \tag{6}$$

While in thermal neutron scattering $\Psi^s(q,\omega)=2\pi\delta(\omega)$, making the recoilless incoherent scattering also elastic, this is not so in general. A well-known example is the Mössbauer absorption experiment, for which $q=k_0$ and $\omega=ck_0(1+v/c)\neq 0$ if $\hbar k_0$ is the momentum of the absorbed incoming γ quantum, c the velocity of light in vacuum, and v/c the small relative frequency shift produced by the moving γ source. Obviously, a detector behind the absorber would give a counting rate

$$Z(v) \propto \left[\text{const}' - \frac{d^2\sigma}{d\Omega d\omega}\right]_{\omega=ck_0(1+v/c)}$$
$$\propto [\text{const} - f_s(q)\Psi^s(q,(c+v)k_0)] \tag{7}$$

if s denotes the particle species which consists of the Mössbauer nuclei. The Doppler shift vk_0 produced by the moving source is so small that the other terms in the total cross section do not vary with v appreciably ($-v_{\max}\leq v\leq v_{\max}$ and $v_{\max}$ of order 10^{-3} ms^{-1}) and are, therefore, included in the constant term in Eq. (7) [$\Delta\omega\simeq v_{\max}k_0=10^{-3}$ ms^{-1}(14.4/$\hbar c$) keV for Fe^{57}, for example]. From the above it is clear that the long-time limit of the tagged-particle relaxation function, $f_s(q)$, is simply the LMF of particle of species s.

C. Mode-coupling equations for LMF's

Using the Mori-Zwanzig formalism[15] and adopting the procedure used for Debye-Waller factors (DWF) in paper I, the generalized oscillator equation for the tagged-particle density-relaxation function in the $t\to\infty$ limit[9,14] reduces to

$$v_s^2 q^2 f_s(q) + \tilde{K}_s(q)[f_s(q)-1]=0 \ . \tag{8}$$

Here v_s denotes the particle's thermal velocity ($v_s^2=k_BT/m_s$, m_s the mass of particles of species s). Applying MCT to the friction kernel $\tilde{K}_s(q)$ we find for a two-component system $\tilde{K}_s(q)=v_s^2K_s(q)$,

$$K_s(q)=1/(N_sq^2)\sum_{i,j}\sum_{\mathbf{k}} f_s(|\mathbf{q}-\mathbf{k}|)(\mathbf{k}\cdot\mathbf{q})^2\tilde{C}_{si}(k)\tilde{C}_{sj}(k)$$
$$\times[S_{ii}(k)S_{jj}(k)]^{1/2}f_{ij}(k) \ , \tag{9a}$$

where according to Eq. (8)

$$f_s(q)=1/[1+q^2/K_s(q)] \ . \tag{9b}$$

Here $\tilde{C}_{ss'}(k)$ are the direct-pair-correlation functions whose explicit expressions are given in paper I and $S_{ss'}(k)=[I-\tilde{C}(k)]^{-1}_{ss'}$ denotes the partial structure factors. Note that K_s has an explicit linear dependence on the LMF's, while in paper I we saw that $K_{ss'}$ depends bilinearly on $f_{ss'}(q)$. Unlike the nonergodicity parameters $f_{ss'}(q)$, which are strongly interdependent through highly nonlinear equations, the LMF's $f_s(q)$ are solved separately for species 1 and 2. The latter are only indirectly coupled via the static structure factors and the nonergodicity parameters entering Eqs. (9) as input information.

III. NUMERICAL RESULTS

The nonlinear Eqs. (9) have been solved for LMF's self-consistently for various values of the system parameters η, δ, and c_1.

A. Glass instability

In this subsection we consider the solutions of Eq. (9) for $c_1=0.9$, $\delta=0.2$ as η is varied from $\eta=0.57$ to 0.51. We find nonzero solutions $f_2(q)>0$ for $\eta\geq 0.52$ (see Fig. 1) while $f_2(q)\equiv 0$ for the lowest density $\eta=0.51$ due to vanishing coherent input parameters $f_{ij}(q)$. Thus for $\eta>\eta_c$ ($0.51<\eta_c<0.52$) the big particles are localized, forming a glassy matrix in which the small particles move (localized or delocalized, see below). The shape of LMF of the big particles is very nearly Gaussian. This is demonstrated by plotting $\ln[f_2(q)]$ as a function of q^2 (Fig. 2) or, more clearly, in Fig. 3, where we show the q-dependent generalized localization length of the large particles

$$l_2(q)=[2/K_2(q)]^{1/2} \ , \tag{10}$$

in comparison to the same quantity (shown by dashed lines for two η values) for a purely Gaussian LMF,

$$l_2(q)|_{\rm Gaussian}=(2\{\exp[q^2l_2(0)^2/2]-1\}/q^2)^{1/2} \ . \tag{11}$$

Figure 4 shows the variation of $l/l_2(q)$ with respect to η for a representative q value. It is interesting to note that the inverse localization length varies *linearly* with η in the whole range of calculations. The slope of this straight line can be understood by generating an iterative

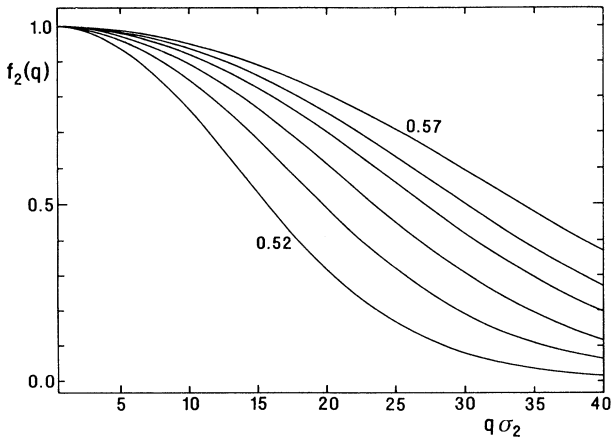

FIG. 1. Lamb-Mössbauer factor $f_2(q)$ of a big particle for total packing fraction $\eta=0.52$, 0.53, 0.54, 0.55, 0.56, and 0.57 at fixed $\delta=\sigma_1/\sigma_2=0.2$ and $c_1=N_1/(N_1+N_2)=0.9$. The sequence of curves is that of the η list.

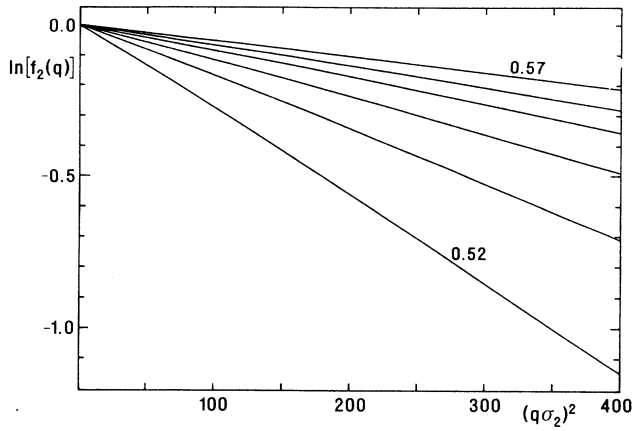

FIG. 2. $\ln[f_2(q)]$ vs $(q\sigma_2)^2$. All parameters as in Fig. 1.

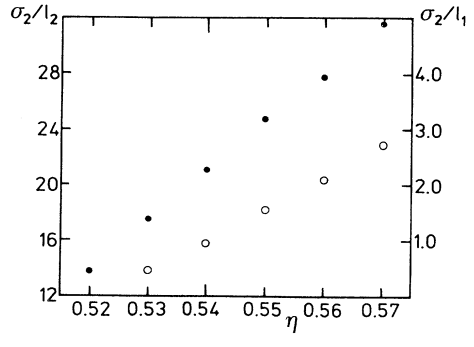

FIG. 4. Inverse localization lengths $l/l_2(q)$ (solid circles) and $l/l_1(q)$ (open circles) vs η at fixed $q\sigma_2=0.4$, $c_1=0.9$, and $\delta=0.2$. [$l_s(q)$ is measured in units of σ_2].

solution of Eq. (9) starting from the strong-friction limit $f_s(q)=1$, i.e., $K_s(q)^{(0)}=\infty$, according to

$$K_s(q)^{(n)}=K_s(q)^{(1)}-\sum_{\mathbf{k}}F_s(\mathbf{q};\mathbf{q}-\mathbf{k})k^2/[k^2+K_s(k)^{(n-1)}],$$

$$s=2\ . \qquad (12)$$

Here

$$F_s(\mathbf{q};\mathbf{k})$$

$$=1/(q^2N_s)\sum_{i,j}(\mathbf{k}\cdot\mathbf{q})^2\tilde{C}_{si}(k)\tilde{C}_{sj}(k)[S_{ii}(k)S_{jj}(k)]^{1/2}f_{ij}(k)$$

and $K_s(q)^{(1)}=\sum_{\mathbf{k}}F_s(\mathbf{q};\mathbf{q}-\mathbf{k})$ is independent of $\mathbf{q}$. Figure 5 demonstrates the behavior of the first ($n=1$), second ($n=2$), and converged ($n\to\infty$) solution of Eq. (12). It is clear from this comparison that the linear slope of $\sqrt{K_2(q)}$ found as a function of η in our calculations reflects this same linear behavior of the strong-friction limit. Note that the second term in Eq. (12) only contributes a correction $\leq 25\%$ to the strong-friction limit. Due to extremely slow convergence, our calculations have not been carried out sufficiently close to the glass-transition point η_c to observe the expected asymptotic $\sqrt{\eta-\eta_c}$ behavior. Such nonanalytic behavior of the solution of Eq. (9) will result from the $\sqrt{\eta-\eta_c}$ asymptotic form of the coherent input $f_{ij}(q)$ (see paper I and Ref. 7).

Turning to the small particles' properties, Fig. 6 shows the LMF's $f_1(q)$ for various η which differ qualitatively from the $f_2(q)$. While for $\eta>\eta_A>\eta_B$ ($0.52<\eta_A<0.53$) the small particles are localized (though with a much longer localization length than the big particles), they get delocalized, i.e., they are diffusing through the glassy matrix of big particles for $\eta\leq\eta_A$. This phenomenon, which was first predicted in Ref. 9, has recently been observed in a computer simulation[16] of a binary mixture of Lennard-Jones particles. As temperature was decreased, the system showed a glass transition at $T=T_B$, indicated by an abrupt strong decrease of the diffusion constant of the big particles, while the small particles' diffusion constant remained liquidlike until it dropped to a small value of hopping diffusion at temperature $T_A<T_B$. Within the classification of ergodic-to-nonergodic transitions given by Götze,[3] the delocalization transition is of type A, while the glass transition corresponds to a type-B transition. This explains our choice of notations above. It is interesting to note that the partial packing fraction of small particles $[\eta c_1\delta^3/(c_1\delta^3+c_2-\eta c_2)=0.071$ at

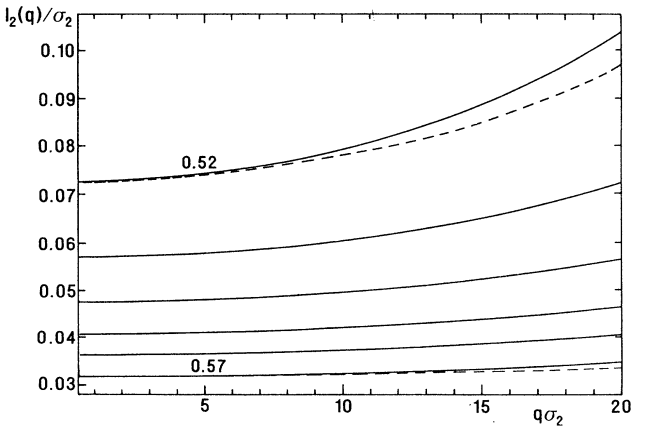

FIG. 3. Generalized localization length $l_2(q)$ of a big particle (measured in units of σ_2). All parameters as in Fig. 1. Dashed lines are the Gaussian approximation, Eq. (11), to $l_2(q)$ for $\eta=0.52$ and 0.57.

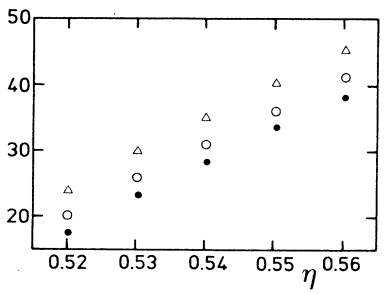

FIG. 5. Iterative solutions of Eq. (12), $[K_2^{(n)}(q)\sigma_2^2]^{1/2}$, for $n=1$ (triangles), $n=2$ (open circles) and $n=\infty$ (solid circles). All parameters as in Fig. 4.

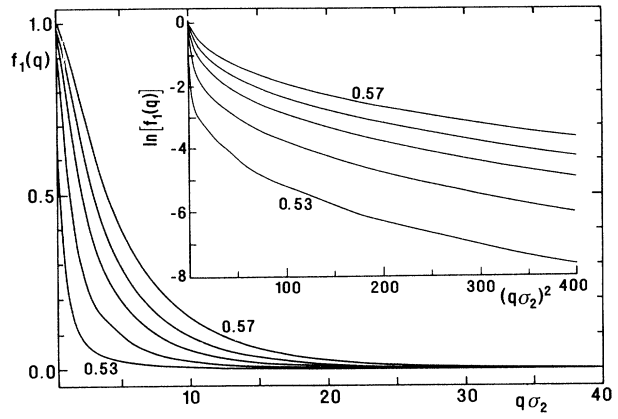

FIG. 6. Lamb-Mössbauer factor $f_1(q)$ of a small particle for total packing fraction $\eta=0.53$, 0.54, 0.55, 0.56, and 0.57 at fixed $\delta=0.2$ and $c_1=0.9$. Inset shows $\ln[f_1(q)]$ vs $(q\sigma_2)^2$. The sequence of curves is that of the η list.

$\eta=0.57$, $\delta=0.2$, and $c_1=0.9$] is so low that it would correspond to a dilute liquid (for hard spheres) if the interaction with the big particles were not present. However, strong long-range indirect interactions mediated via the big particles localize the small particles even at such low densities. Classification of a low-density charged hard-sphere liquid has been reported recently,[17] and it is, of course, also the long-range of Coulomb interactions which is responsible for the glass forming in that system.

A second characteristic difference in the LMF's of small and big particles is the continuous decrease to zero of the inverse localization length as the delocalization point $\eta=\eta_A$ is approached (Fig. 4). Figure 7 shows the generalized q-dependent localization length $l_1(q)$, which exhibits an interesting dip at wave vector q_0 [q_0 is the position of the main peak in $S_{22}(q)$], the physical significance of which can be understood from the probability density function $P_1(r)=4\pi r^2 f_1(r)$. In Fig. 8, $P_1(r)$ (solid line) and

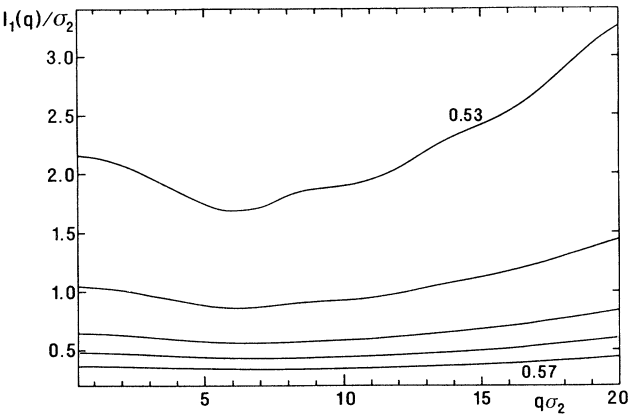

FIG. 7. Generalized localization length $l_1(q)$ of a small particle (measured in units of σ_2). All parameters as in Fig. 6.

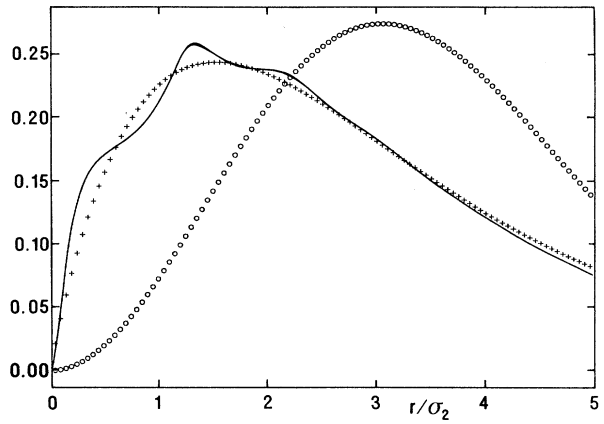

FIG. 8. Probability density $P_1(r)$ (solid curve), $P_1^0(r)$ (crosses), and $P_1^G(r)$ (open circles) for fixed $\eta=0.53$, $c_1=0.9$, and $\delta=0.2$.

$$P_1^0(r)=\frac{2r}{l_1^2(0)}\exp\left[\frac{-\sqrt{2}}{l_1(0)}r\right] \tag{13a}$$

(crosses) are plotted for $\eta=0.53$, where particles are about to delocalize. Here $P_1^0(r)$ is obtained by approximating $K_1(q)\simeq K_1(0)=2/l_1^2(0)$ in Eq. (9), i.e.,

$$f_1(q)\simeq 1/[1+\tfrac{1}{2}q^2 l_1^2(0)]\ . \tag{13b}$$

In addition, Fig. 8 shows the Gaussian probability distribution (open circles)

$$P_1^G(r)=4\pi r^2\exp\{-r^2/[2l_1^2(0)]\}/[2\pi l_1^2(0)]^{3/2}\ . \tag{13c}$$

In order to emphasize the non-Gaussian character of the motion of the small particles. Obviously, the anharmonic thermal motion of the small particles with large localization is much better approximated by the expression Eq. (13a) than the conventional assumption of a Gaussian probability distribution, Eq. (13c). The position $r_{\max}$ of the broad maximum in Fig. 8 is determined by the localization length $l_1(0)$ and given by $r_{\max}=l_1(0)/\sqrt{2}$ [according to Eq. (13a)], while the oscillations of $P_1(r)$ around the approximate distribution $P_1^0(r)$ reflect the structure of the glassy matrix, with the oscillation length being roughly equal to the diameter of the big particles.

Turning to Fig. 4, again we note that the η interval covered in our calculations is so small that essential deviations from a linear η dependence of $l_1^{-1}(q)$ are not observed. In contrast to the localization length of the big-particles, where $l_2^{-1}(q)$ could be understood in terms of the strong-friction limit $l_2^{-1}(0)\approx(K_2^{(1)})^{1/2}$, $l_1^{-1}(0)$ is small compared to $[K_1^{(1)}(0)]^{1/2}$ and thus cannot be approximated by the strong-friction expressions. In spite of $(K_1^{(1)})^{1/2}$ being about ten times as large as $l_1^{-1}(0)$, both quantities vary linearly with the same slope as η is changed. This observation, makes unlikely the possibility that the straight-line behavior of $l_1^{-1}(0)$ is an artifact due to an infrared singularity to be discussed below.

B. Concentration dependence of LMF's

The influence of concentration variations on LMF's has been studied by varying c_1 from 0.1 to 0.9 at fixed $\eta=0.55$ and $\delta=0.2$. In Fig. 9, $f_1(q)$ and $f_2(q)$ are plotted for various c_1. First, it is to be noted that the half-widths of LMF's for large and small particles differ by a factor of about 8, indicating a correspondingly large difference in their localization lengths. Secondly, the trend in the variation of the widths as c_1 is increased is opposite. While the localization length of the big particles is decreased [increasing width of $f_2(q)$], the small particles exhibit a slight increase in their localization length as c_1 is varied from 0.1 to 0.9.

The behavior of the localization length of the big particles (Fig. 10) seems quite plausible because we expect these particles to become more and more confined by the small particles as $c_1\to 1$. More precisely, we expect $l_2(c_1\to 1)/\sigma_2\approx 0.05\delta$, since from Fig. 3 of Ref. 2 we conclude that for a hard-sphere one-component system at $\eta=0.55$, $l/\sigma\approx 0.05$. The opposite limiting value for $c_1\to 0$ $[l_2(c_1\to 0)/\sigma_2\approx 0.05]$ is almost reached at $c_1=0.1$. The reason for l_2 staying essentially constant up to about $c_1=0.7$ can be traced back to the almost constant partial packing fraction $\eta_2=\eta c_2/(c_1\delta^3+c_2)$ in the range $0.1<c_1<0.7$.

Turning back to the LMF of the small particles (Fig. 9), these particles exhibit strongly anharmonic motions with large localization lengths. This is demonstrated in Fig. 11. Due to the large values of $l_1(q)|_{\text{Gaussian}}$, Eq. (11) increases rapidly with increasing q, falling outside the frame of Fig. 11 for $q\sigma_2\geq 6$. It is interesting to note that the trend of an increasing localization length l_1 with increasing concentration must be reversed in the small interval $0.9<c_1<1$, since we expect $l_1(c_1\to 1)/\sigma_2=0.05$, according to the above argument. The onset of this decrease of l_1 can be observed by the weaker q dependence of $l_1(q)$ (Fig. 11) for $c_1=0.9$.

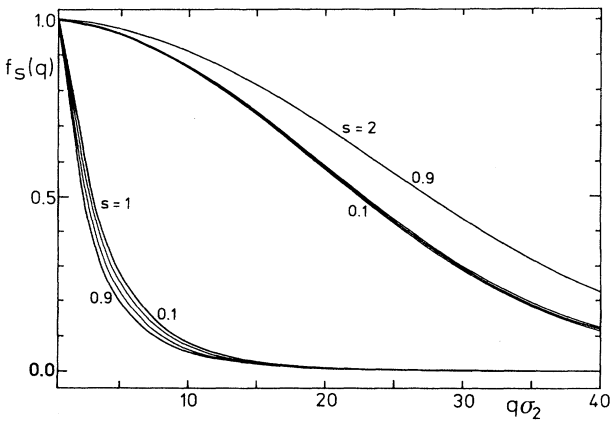

FIG. 9. Lamb-Mössbauer factors of big particles $[f_2(q)]$ and small particles $[f_1(q)]$ for $c_1=0.1$, 0.3, 0.5, 0.7, and 0.9 and fixed $\delta=0.2$, $\eta=0.55$. For small particles the sequence of curves is from right to left according to the c_1 list, while for big particles it is the opposite.

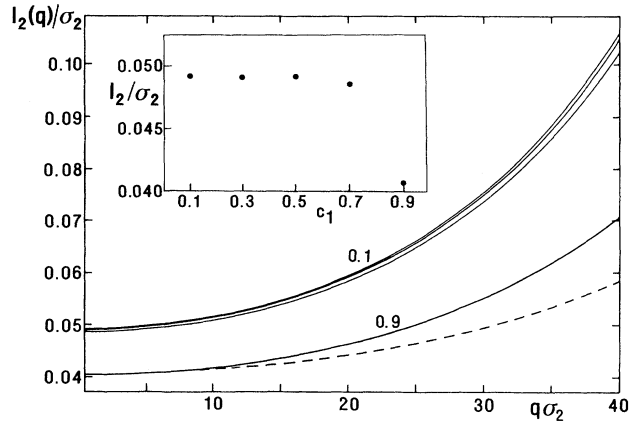

FIG. 10. Generalized localization length $l_2(q)$ for a big particle (measured in units of σ_2). All parameters as in Fig. 9. The dashed line at $c_1=0.9$ is the Gaussian approximation, Eq. (11), to $l_2(q)$. The inset shows $l_2(q=0.4)/\sigma_2$ vs c_1.

Figure 12 shows for $c_1=0.1$ and 0.9 information about the detailed spatial distribution of the small particles which is contained in the q dependence of $f_1(q)$ or, equivalently, in $l_1(q)$. The common features of $P_1(r)$, which remain invariant with concentration (see inset, Fig. 12), are the small shoulder at $r=1{\cdot}2\sigma_2$, in addition to the first broad peak at around $r\approx 0{\cdot}3\sigma_2$. These features can be understood if we recall Fig. 8, where $P_1(r)$ was shown for lower density ($\eta=0.53$, $c_1=0.9$, and $\delta=0.2$). Due to an increase in density accompanied by a stronger localization of the particles, the small-r shoulder of $P_1(r)$ in Fig. 8 evolves to a pronounced peak in Fig. 12, while the central peak of Fig. 8 reduces to a shoulder in Fig. 12, suggesting that small particles still get a chance to go around a big particle once in a while. In contrast, for $\eta=0.53$ this is a most frequent event, making $r\approx 1.3\sigma_2$ the most probable distance to find the small particle for $t\to\infty$. A somewhat related feature is the appearance of a shoulder, which has been seen very recently in a molecular-dynamics simulation by Raux *et al.*[18] Howev-

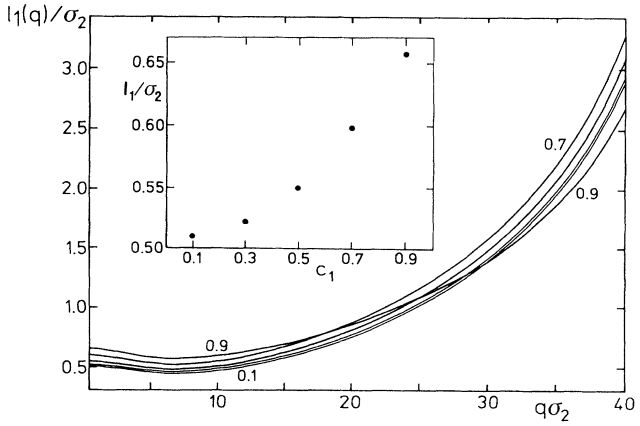

FIG. 11. Generalized localization length $l_1(q)$ for a small particle. Other details as in Fig. 10.

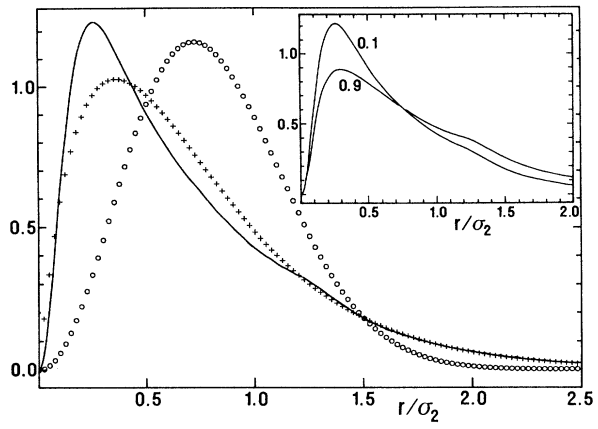

FIG. 12. Probability density $P_1(r)$ (solid curve), $P_1^0(r)$ (crosses), and $P_1^G(r)$ (open circles) for fixed $\eta=0.55$, $c_1=0.1$, and $\delta=0.2$. Inset shows $P_1(r)$ for $c_1=0.9$ in comparison to $P_1(r)$ at $C_1=0.1$.

er, the small peak in their $4\pi r^2 G_s^1(r,t)$ [$G_s^1(r,t)$ is the self-density autocorrelation function] at around $1.0\sigma_1$ has been traced back to activated processes allowing the particles to jump into the interstitial sites of the disordered system. It is also clear from Fig. 12 that there is stronger localization of the small particles when their concentration is increased. This fact is seen through the increase in the first peak height and its shift towards smaller distance.

C. Size-ratio dependence of LMF's

Figure 13 shows $f_2(q)$ for $\eta=0.55$, $c_1=0.5$, and various size ratios δ. At high packing fraction, the big particles are strongly localized at all δ and form a rigid glassy matrix, even when the small particles get delocalized[9] for $\delta\leq 0.14$. The big particles' LMF can be well represented by Gaussians (see inset, Fig. 13; for deviations from Gaussian, see Sec. III A) with mean-square displacements $u^2=\frac{1}{2}l_2^2(0)$ increasing slightly with decreasing δ. Thus,

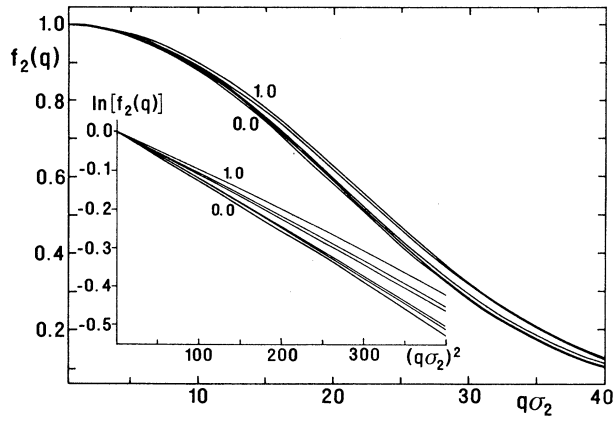

FIG. 13. Lamb-Mössbauer factor $f_2(q)$ of a big particle for $\delta=0.0$, 0.1, 0.2, 0.3, 0.4, 0.5, and 1.0 at fixed $c_1=0.5$ and $\eta=0.55$. The inset shows $\ln[f_2(q)]$ vs $(q\sigma_2)^2$. The sequence of curves is that of the δ list.

inclusion of small particles into the voids of a glassy matrix produces a destabilizing effect on the rigid matrix.

In contrast to the behavior of the big particles, the localization length of the small particles changes drastically with increasing δ (Figs. 14 and 15). Also, Fig. 14, as well as Fig. 2(a) of Ref. 9, clearly displays a continuous transition from a nearly Gaussian ($\delta=1$) to a highly non-Gaussian ($\delta=0.2$) form of $f_1(q)$. It is interesting to note that the mode-coupling equations, Eq. (9), correctly account for the expected change from nearly harmonic oscillations of localized particles ($\delta=1.0$ and $\eta=0.55$) to the very anharmonic motion of small particles in the voids of a frozen matrix. Figure 15 shows that the localization length l_1 of small particles increases *continuously* as δ approaches a critical value δ_c ($0.1<\delta_c<0.2$), where l_1 becomes infinite. The detailed behavior of l_1 close to the delocalization transition is marred by an infrared singularity[19,20] which dominates the solution of Eq. (9) for sufficiently large l_1. It is responsible for an asymptotic linear dependence $l_1^{-1}\propto\epsilon=\delta/\delta_c-1$, which seems to prevail in our numerical calculations up to $\delta\approx 0.3$ (see inset Fig. 15). The infrared singularity can be avoided[21] by postulating a wave-number-independent friction kernel in Eq. (9), $K_1(q,\epsilon)=K_1(\epsilon)$, and solving Eq. (9) for $q=0$:

$$1=\sum_{\mathbf{k}} F_1(\mathbf{q};\mathbf{k})\frac{1}{k^2+K_1(\epsilon)}\ , \tag{14}$$

which results in

$$K_1(\epsilon)=\epsilon\left[\int_0^\infty dk\, k^2\frac{d}{d\epsilon}F(k,\epsilon)\bigg|_{\epsilon=0}\Big/\int_0^\infty dk\, F(k,0)\right] \tag{15}$$

with

$$F(k,e)=\sum_{i,j}\tilde{C}_{1i}(k)\tilde{C}_{1j}(k)[S_{ii}(k)S_{jj}(k)]^{1/2}f_{ij}(k)$$

for $\epsilon\rightarrow 0$. The solutions of Eq. (15) are also shown in Fig. 15 (triangles). Equations (15) and (16) imply the critical behavior $l_1^{-1}\propto\epsilon^{1/2}$, which is the same as for a Lorentz particle,[21] and this is clearly exhibited by the numerical

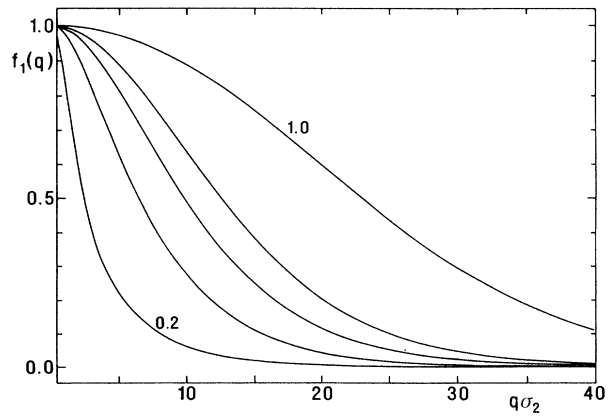

FIG. 14. Lamb-Mössbauer factor $f_1(q)$ of a small particle for $\delta=0.2$, 0.3, 0.5, 0.5, and 1 at fixed $c_1=0.5$ and $\eta=0.55$. The sequence of curves is that of the δ list.

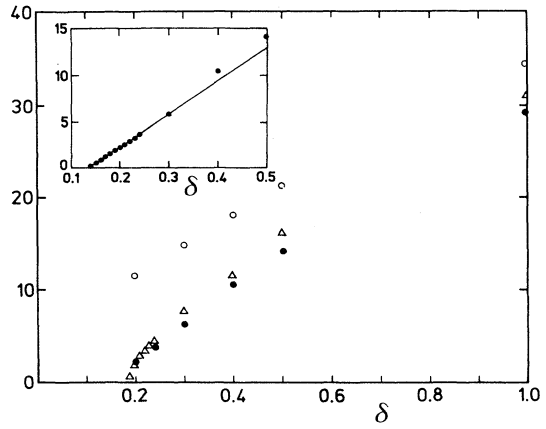

FIG. 15. Inverse localization length $1/l_1(q)$ vs δ at fixed $q=0.4$, $c_1-0.5$, and $\eta=0.55$. Solid circles: solution of Eq. (9): triangles: solution of Eq. (14); open circles: strong-friction limit solution of Eq. (12). The inset shows $1/l_1(q)$ according to Eq. (9) near the delocalization. [$l_1(q)$ is measured in units of σ_2).]

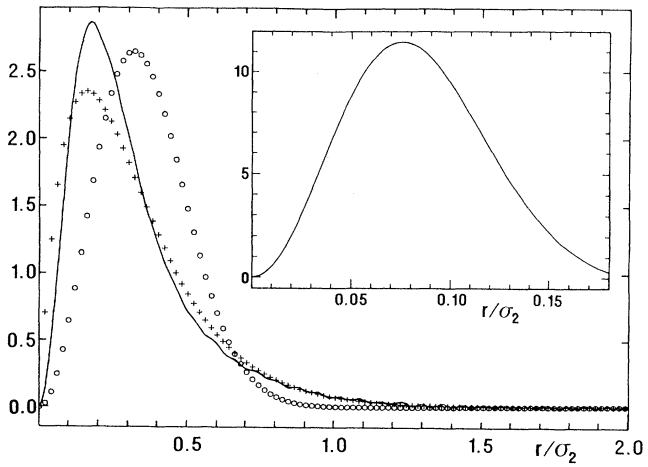

FIG. 16. Probability density $P_1(r)$ (solid curve). $P_1^0(r)$ (crosses), and $P_1^G(r)$ (open circles) for fixed $\eta=0.055$, $c_1=0.5$, and $\delta=0.3$. Inset shows for comparison $P_1(r)$ at $\delta=1.0$.

solutions (Fig. 15) with $\delta_c\approx 0.18$. Note that for $\delta>0.2$ the solutions of Eqs. (9) and (15) are rather similar. Therefore, we think that the calculated $K_1(q)$ gives a reasonable picture of reality, although the nearly linear increase of $\sqrt{K_1(q)}$ for $0.14<\delta<0.3$ should not be taken seriously, since it is an artifact of infrared singularity with no physical relevance.

In our opinion, it is important to keep the q dependence in the friction kernel of small particles, since it describes physically plausible structural features of the glassy matrix (see Fig. 8). In this sense, Eq. (15) considerably overestimates $K_1(q)$ for $\delta>0.25$ (Fig. 15). However, close to the delocalization transition the approximation Eq. (15) is to be preferred for the reason discussed above. Near $\delta=1$ the results for $K_1(q)$ may be understood by the strong-friction limit expression Eq. (12) according to the argument in Sec. III A. This limit is indicated in Fig. 15 by open circles.

Finally, Fig. 16 shows the probability distribution for $\delta=0.3$ and for a comparison, an inset with $P_1(r)$ for $\delta=1$. Nearly harmonic behavior of the particles at $\delta=1$ is very clearly seen by the nearly dumb bell structure of $P_1(r)$. There is only a small deviation from the Gaussian, as is marked by the shift in the position of the maximum [$r_{\max}=l_1(0)\sqrt{2}=0.071\sigma_2$ for purely Gaussian distribution]. As δ is decreased, the increased localization length is clearly exhibited by $P_1(r)$, which is now better approximated by Eq. (13a) rather than a Gaussian. At $\delta=0.3$, the probability distribution of the small particles does not yet reflect the same detailed structure of the glassy matrix as was seen for $\delta\equiv 0.2$ (Fig. 8). However, the long tail of $P_1(r)$ points out the fact that the particle is making long-distance excursions.

IV. SUMMARY AND CONCLUSIONS

The implications of the glass transition (paper I) in a binary mixture of hard spheres, on the long-time limits of the tagged-particle density-relaxation functions (LMF's) has been studied within mode-coupling theory. We calculated the wave-number-dependent LMF's for both species at various system parameters. As long as particles of both species have similar size, we find that the liquid-glass transition is associated with the localization of all particles in the system. The localization length drops discontinuously from infinity (liquid) to a finite value (glass), which is consistent with Lindemann's melting criterion. If the diameter ratio is chosen sufficiently small, a new phenomenon will appear. While the big particles are localized at the glass-transition point as discussed above, the small particles will keep their mobility and diffuse through the voids of the glassy matrix. On increasing the packing fraction further (see Sec. III A), the diffusion will be blocked, and the small particles become localized in a type-A transition.

The wave-number dependence of the LMF of the big particles is well represented by a Gaussian for all η down to the glass-liquid transition point reflecting small-amplitude oscillations in a harmonic potential. In contrast, the LMF of the small particles has a characteristic non-Gaussian form. The outstanding feature of this LMF is that its values in the large-q wing are much larger than those of a Gaussian of corresponding localization length. Physically, this result of our calculation reflects the motion of the small particles in "channels" which are determined by the anharmonic potential set up by the glassy matrix.

ACKNOWLEDGMENTS

We thank Professor A. Sjölander, Professor W. Götze, and Dr. L. Sjogren for helpful discussions. This work is supported by Deutsche Forschungsgemeinschaft (DFG) Grant No. Bo 873/1-1.

[1]E. Leutheusser, Phys. Rev. A **29**, 2765 (1984).
[2]U. Bengtzelius, W.Götze, and A. Sjolander, J. Phys. C **17**, 5915 (1984).
[3]W. Götze, Z. Phys. B **56**, 139 (1984); H. De Raedt and W. Götze, J. Phys. C **19**, 2607 (1986).
[4]T. R. Kirkpatrick, Phys. Rev. A **31**, 939 (1985).
[5]U. Bengtzelius, Phys. Rev. A **34**, 5059 (1986); **33**, 3433 (1986).
[6]W. Götze and L. Sjogren, J. Phys. C **20**, 879 (1987); Z. Phys. B **65**, 415 (1987).
[7]W. Götze, Z. Phys. B **60**, 195 (1985).
[8]J. Bosse and U. Krieger, J. Phys. C **19**, 1609 (1986).
[9]J. Bosse and J. S. Thakur, Phys. Rev. Lett. **59**, 998 (1987).
[10]U. Krieger and J. Bosse, Phys. Rev. Lett. **59**, 1601 (1987).
[11]S. P. Das, G. F. Mazenko, S. Ramaswamy, and J. J. Toner, Phys. Rev. Lett. **54**, 118 (1985).
[12]J. J. Ullo and S. Yip, Phys. Rev. Lett. **54**, 1509 (1985); T. Kinell and S. W. Lovesey, J. Phys. C **19**, 791 (1986).
[13]B. Bernu, J. P. Hansen, Y. Hiwatari, and G. Pastore, Phys. Rev. A **36**, 4891 (1987).
[14]J. Bosse, in *Static and Dynamic Properties of Liquids*, edited by M. Davidovic and A. K. Soper, Springer Proceedings in Physics Vol. 40 (Springer-Verlag, Berlin, 1989), pp. 108–117.
[15]H. Mori, Prog. Theor. Phys. **33**, 429 (1965); **34**, 399 (1965); R. Zwanzig, in *Lectrures in Theoretical Physics*, edited by W. Britten and L. Dunham (Wiley-Interscience, New York, 1961), Vol. 3, p. 135.
[16]M. Ronchetti and J. Bosse (unpublished).
[17]J. S. Thakur and J. Bosse, J. Non-Cryst. Sol. **117/118**, 898 (1990).
[18]J. N. Raux, J. L. Barrat, and J. P. Hansen, J. Phys. Condens, Matter **1**, 7171 (1989).
[19]W. Götze (private communication).
[20]Roger F. Loring and S. Mukamel, J. Chem. Phys. **85**, 1950 (1986).
[21]W. Götze, E. Leutheusser, and S. Yip, Phys. Rev. A **23**, 2634 (1981); **24**, 1008 (1981).